Static interface profiles for contact lines on an elastic membrane with the Willmore energy

Zhen Zhang[*]

Department of Mathematics, Guangdong Provincial Key Laboratory of Computational Science and Material Design,
Southern University of Science and Technology (SUSTech), Shenzhen 518055, People's Republic of China

Jin Yao [†] and Weiqing Ren [‡]

Department of Mathematics, National University of Singapore, Singapore 119076

We consider a fluid interface in contact with an elastic membrane and study the static profiles of the interface and the membrane. Equilibrium conditions are derived by minimizing the total energy of the system with volume constraints. The total energy consists of surface energies and the Willmore energy; the latter penalizes the bending of the membrane. It is found that, while the membrane is locally flat at the contact line with the contact angle satisfying the Young-Dupré equation, the gradient of the mean curvature of the membrane exhibits a jump across the contact line. This jump balances the surface tension of the fluid interface in the normal direction of the membrane. Asymptotic solutions are obtained for two-dimensional systems in the limits as the reduced bending modulus ν tends to $+\infty$ and 0, respectively. In the stiff limit as $\nu \to +\infty$, the leading-order solution is given by that of a droplet sitting on a rigid substrate with the contact angle satisfying the Young-Dupré equation; in contrast, in the soft limit as $\nu \to 0$, a transition layer appears near the contact line and the interfaces have constant curvatures in the outer region with apparent contact angles obeying Neumann's law. These solutions are validated by numerical experiments.

I. INTRODUCTION

We consider a system consisting of two immiscible fluids in contact with a substrate. A liquid droplet sitting on a substrate is such an example. Three interfaces are present in the system: one between the two fluids and the other two between the fluids and the solid. The line where the three interfaces meet is called the contact line.

The static profiles of the interfaces can be obtained by minimizing the total energy of the system. Consider for example the energy due to surface tensions only,

$$F = \sum_{i=1}^{3} \gamma_i |\Sigma_i|, \quad (1)$$

where Σ_i $(i = 1, 2)$ are the interfaces between the fluids and the substrate, Σ_3 is the interface between the two fluids, γ_i $(i = 1, 2, 3)$ are the interfacial tension coefficients, and $|\Sigma_i|$ $(i = 1, 2, 3)$ denote the areas of the interfaces. We distinguish two cases: a rigid substrate and a soft substrate. In the case of rigid substrate, the minimization of the energy (1) with the constant volume constraint for the droplet yields a constant curvature for the droplet surface and the Young-Dupré equation for the contact angle [1]:

$$\gamma_3 \cos \theta_Y = \gamma_2 - \gamma_1, \quad (2)$$

where θ_Y is the angle between the fluid interface and the substrate. This equation is simply the force balance in the tangential direction of the substrate. When the substrate is soft, its deformation has to be taken into account, so the energy (1) is minimized with respect to the three interfaces with volume constraints. This yields constant curvatures for the interfaces and a cusplike structure for the substrate at the contact line with the contact angles satisfying Neumann's law [2]:

$$\frac{\sin \theta_{12}}{\gamma_3} = \frac{\sin \theta_{23}}{\gamma_1} = \frac{\sin \theta_{31}}{\gamma_2}, \quad (3)$$

where θ_{ij} is the contact angle between the interfaces Σ_i and Σ_j. Neumann's law describes the force balances in both the tangential and normal directions to the substrate.

Contact lines on deformable substrates have attracted much attention in recent years [3–15]. These works revealed very interesting phenomena, for example, the formation of cusps at the contact line, the stick-slip motion of the contact line, etc. In this work, we consider contact lines on an elastic membrane and study the static profiles of the interfaces. Elastic membranes are widely used in modeling vesicles [16–25] and in the study of fluid-structure interactions in fluid dynamics [26,27]. Those earlier works focused on the interaction of a membrane with a single-phase fluid. When a membrane is in contact with two-phase fluids, it is deformed at the contact line where the fluid interface intersects the membrane. We are particularly interested in the local profiles of the fluid interface and the membrane near the contact line.

The total energy of the system consists of the surface energies as discussed above, and also a contribution from the

[*]zhangz@sustech.edu.cn

[†]yaojin@u.nus.edu

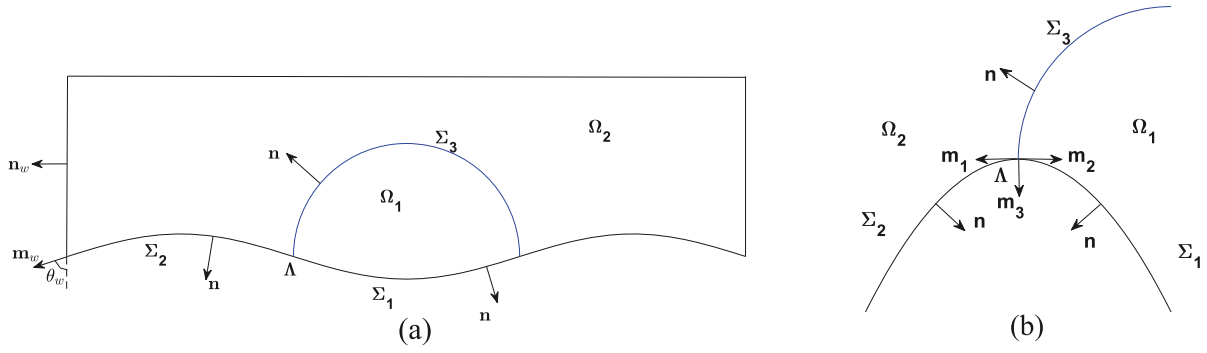[‡]Corresponding author: matrw@nus.edu.sg

FIG. 1. Left panel: Setup of the system consisting of a droplet on a membrane. Right panel: The three interfaces near the contact line.

Willmore bending energy on the membrane. Using calculus of variation, we derive the equilibrium conditions for the profiles of the interfaces. The cusp structure of the membrane mentioned above is regularized by the Willmore energy, so the membrane is locally flat at the contact line. The Young-Dupré equation, which describes the tangential force balance at the contact line, still holds for the contact angle. However, the gradient of the mean curvature of the membrane exhibits a jump across the contact line. This produces a force which balances the surface tension of the fluid interface in the normal direction of the membrane at the contact line.

The strength of the bending energy is characterized by a parameter called the bending modulus. We compute the asymptotic solutions for the interface profiles in the limits as the reduced bending modulus tends to $+\infty$ and 0. The former corresponds to a stiff membrane, and the latter corresponds to a soft membrane. In the stiff limit, the regular perturbation applies and the leading-order solution is that of a spherical droplet sitting on a rigid substrate, with the contact angle satisfying the Young-Dupré equation. In the soft limit, however, a transition layer appears near the contact line. Using matched asymptotic analysis, we find that, though the microscopic contact angle in the inner region satisfies the Young-Dupré equation, the apparent contact angles between the three interfaces in the outer region obey Neumann's law.

We also propose a finite-difference numerical method to compute the static interface profiles. The governing equations are highly nonlinear, so we use a gradient flow to evolve the system and compute the steady-state solution which gives the static interface profiles. A semi-implicit scheme is used for the temporal discretization to improve the numerical stability. We find that the numerical results for the interface profiles and the apparent contact angles agree very well with the asymptotic solutions.

The paper is organized as follows. In Sec. II, we present the total energy of the system and derive the governing equations for the interfaces and the conditions at the contact line. Sections III and IV are devoted to the asymptotic analysis of the mathematical model in the limits as the reduced bending modulus tends to $+\infty$ and 0, respectively. In Sec. V, we propose the semi-implicit finite difference numerical method and present numerical results. The paper is concluded in Sec. VI. Details for the calculus of variation employed in the derivation of the governing equations are provided in the Appendices.

II. GOVERNING EQUATIONS

We consider a droplet sitting on an elastic membrane, as shown in Fig. 1 (left panel). The membrane is denoted by Ξ, which consists of Σ_1, Σ_2, and the contact line Λ. The droplet surface is denoted by Σ_3. The whole system is confined in a rigid box, where the membrane meets with the vertical side walls of the box at the lines denoted by $\partial\Xi$. We use Ω_1 and Ω_2 to denote the the domain occupied by the droplet and the domain outside the droplet, respectively. We assume the volumes Ω_1 and Ω_2 are both conserved. The unit normal vectors to Σ_i ($i = 1, 2, 3$) are denoted by $\mathbf{n}$, where it points outside the domain $\Omega_1 \cup \Omega_2$ on the membrane and points from Ω_1 to Ω_2 on the droplet surface. The unit normal vector to the wall is denoted by $\mathbf{n}_w$.

The energy of the system is given by

$$F = \sum_{i=1}^{3} \int_{\Sigma_i} \gamma_i dA + \frac{c_b}{2} \int_{\Xi} H^2 dA. \qquad (4)$$

The first term on the right-hand side of the above equation represents the interfacial energies, with γ_i ($i = 1, 2, 3$) being the interfacial tension coefficient on the respective interface. The second term, which is known as the Willmore energy, models the bending energy of the membrane, with c_b being the bending modulus and H the mean curvature of Ξ.

This term is also named the Helfrich energy [28] and is widely used in modeling vesicle dynamics in fluids. Since our focus is on the interface profiles near the contact line Λ, for simplicity we have assumed that the interfacial energies between the wall and the fluids above and below the membrane are the same, so they did not appear in (4).

The static profiles of the droplet and the membrane are obtained by minimizing the total energy, under the constraints that the volumes of Ω_1 and Ω_2 are conserved,

$$\int_{\Omega_i} d\mathbf{x} = V_i, \quad i = 1, 2. \qquad (5)$$

Introducing the Lagrange multipliers λ_1 and λ_2 for the two constraints respectively, we write the Lagrangian as

$$\mathcal{L} = F - \lambda_1 \left(\int_{\Omega_1} d\mathbf{x} - V_1 \right) - \lambda_2 \left(\int_{\Omega_2} d\mathbf{x} - V_2 \right). \qquad (6)$$

We parametrize the membrane as $\mathbf{q}(s^1, s^2)$ with $(s^1, s^2) \in D_m$ and the droplet surface as $\mathbf{r}(s^1, s^2)$ with $(s^1, s^2) \in D_s$, where

q and **r** are the position vectors. We assume that the function **q** is smooth everywhere except that, across the contact line, it is only assumed to be continuously differentiable. Thus the normal and tangent vectors of the membrane are continuous across the contact line. We further assume that the contact line is a smooth curve. At the contact line Λ, the droplet surface meets with the membrane, so we have $\mathbf{q} = \mathbf{r}$. The variations of the membrane and the droplet are denoted by $\delta\mathbf{q}$ and $\delta\mathbf{r}$ respectively, where

$$\delta\mathbf{q} = \delta\mathbf{r} \quad \text{on } \Lambda \tag{7}$$

and

$$\delta\mathbf{q} \cdot \mathbf{n}_w = 0 \quad \text{on } \partial\Xi. \tag{8}$$

The first condition ensures the interfaces Σ_3 and Ξ meet at the contact line, and the second condition implies the membrane cannot penetrate into the wall.

The resulting variation of the Lagrangian is calculated as follows. Details of the derivation are provided in Appendix A. First, the variations of the volumes of Ω_1 and Ω_2 are given by the sum of two surface integrals,

$$\delta\int_{\Omega_1} d\mathbf{x} = \int_{\Sigma_1} \delta\mathbf{q} \cdot \mathbf{n}\, dA + \int_{\Sigma_3} \delta\mathbf{r} \cdot \mathbf{n}\, dA, \tag{9a}$$

$$\delta\int_{\Omega_2} d\mathbf{x} = \int_{\Sigma_2} \delta\mathbf{q} \cdot \mathbf{n}\, dA - \int_{\Sigma_3} \delta\mathbf{r} \cdot \mathbf{n}\, dA, \tag{9b}$$

where dA is the differential of surface area. The variation of the area of Σ_1 is given by the sum of a line integral and a surface integral,

$$\delta\int_{\Sigma_1} dA = \int_{\Lambda} \delta\mathbf{q} \cdot \mathbf{m}_1 dl + \int_{\Sigma_1} \delta\mathbf{q} \cdot (2H\mathbf{n})dA, \tag{10}$$

where $\mathbf{m}_1$ is the unit conormal vector to Σ_1 at the contact line (see the right panel of Fig. 1), and dl is the differential of arclength. Similar results hold for the variations of the areas of Σ_2 and Σ_3:

$$\delta\int_{\Sigma_2} dA = \int_{\Lambda} \delta\mathbf{q} \cdot \mathbf{m}_2 dl + \int_{\partial\Xi} \delta\mathbf{q} \cdot \mathbf{m}_w dl$$
$$+ \int_{\Sigma_2} \delta\mathbf{q} \cdot (2H\mathbf{n})dA, \tag{11a}$$

$$\delta\int_{\Sigma_3} dA = \int_{\Lambda} \delta\mathbf{r} \cdot \mathbf{m}_3 dl - \int_{\Sigma_3} \delta\mathbf{r} \cdot (2H\mathbf{n})dA, \tag{11b}$$

where $\mathbf{m}_2 = -\mathbf{m}_1$ and $\mathbf{m}_3$ are the unit conormal vectors to Σ_2 and Σ_3 at the contact line, respectively; $\mathbf{m}_w$ is the unit conormal vector to Σ_2 at the boundary $\partial\Xi$. H in the above equations is the mean curvature of the interfaces, defined as

$$H = \begin{cases} \frac{1}{2}\nabla_s \cdot \mathbf{n} & \text{on } \Sigma_1, \Sigma_2, \\ -\frac{1}{2}\nabla_s \cdot \mathbf{n} & \text{on } \Sigma_3, \end{cases} \tag{12}$$

where ∇_s is the surface gradient operator and the negative sign is due to the fact that **n** points upwards on Σ_3.

Next, we consider the variation of the Willmore energy on Ξ. We compute the variation on Σ_1 and Σ_2 separately. First on Σ_1 we have

$$\delta\int_{\Sigma_1} \frac{c_b}{2}H^2 dA = c_b\int_{\Sigma_1} (-\delta\mathbf{q} \cdot \mathbf{n})\left(\frac{1}{2}\Delta_s H + H(H^2 - K)\right)dA$$
$$+ \frac{c_b}{2}\int_{\Lambda} [-H\mathbf{m}_1 \cdot \nabla_s(\delta\mathbf{q} \cdot \mathbf{n}) + (\delta\mathbf{q} \cdot \mathbf{n})(\mathbf{m}_1 \cdot \nabla_s H) + H^2\delta\mathbf{q} \cdot \mathbf{m}_1]dl, \tag{13}$$

where K is the Gaussian curvature and Δ_s is the Laplace-Beltrami operator. It should be noted that the expression in the integral along the contact line should be interpreted as the directional limit approaching Λ from Σ_1. A similar result can be obtained for the variation on Σ_2,

$$\delta\int_{\Sigma_2} \frac{c_b}{2}H^2 dA = c_b\int_{\Sigma_2} (-\delta\mathbf{q} \cdot \mathbf{n})\left(\frac{1}{2}\Delta_s H + H(H^2 - K)\right)dA$$
$$+ \frac{c_b}{2}\int_{\Lambda} [-H\mathbf{m}_2 \cdot \nabla_s(\delta\mathbf{q} \cdot \mathbf{n}) + (\delta\mathbf{q} \cdot \mathbf{n})(\mathbf{m}_2 \cdot \nabla_s H) + H^2\delta\mathbf{q} \cdot \mathbf{m}_2]dl$$
$$+ \frac{c_b}{2}\int_{\partial\Xi} [-H\mathbf{m}_w \cdot \nabla_s(\delta\mathbf{q} \cdot \mathbf{n}) + (\delta\mathbf{q} \cdot \mathbf{n})(\mathbf{m}_w \cdot \nabla_s H) + H^2\delta\mathbf{q} \cdot \mathbf{m}_w]dl, \tag{14}$$

where the expressions in the line integrals are the directional limits approaching the lines from Σ_2.

Combining these results and using the conditions $\delta\mathbf{q} = \delta\mathbf{r}$ and $\mathbf{m}_1 = -\mathbf{m}_2$ at the contact line Λ, we obtain

$$\delta\mathcal{L} = \sum_{i=1}^{2} \int_{\Sigma_i} (\delta\mathbf{q} \cdot \mathbf{n})\left[2\gamma_i H - c_b\left(\frac{1}{2}\Delta_s H + H(H^2 - K)\right) - \lambda_i\right]dA$$

$$+ \int_{\Sigma_3} (\delta\mathbf{r} \cdot \mathbf{n})(-2\gamma_3 H + \lambda_2 - \lambda_1)dA$$

$$+ \int_{\Lambda} \left[\delta\mathbf{q} \cdot (\gamma_1\mathbf{m}_1 + \gamma_2\mathbf{m}_2 + \gamma_3\mathbf{m}_3) + \frac{c_b}{2}\left(-\mathbf{m}_1 \cdot [H\nabla_s(\delta\mathbf{q} \cdot \mathbf{n})]_2^1 + (\delta\mathbf{q} \cdot \mathbf{n})\mathbf{m}_1 \cdot [\nabla_s H]_2^1\right)\right]dl$$

$$+ \int_{\partial\Xi} \left(\gamma_2\delta\mathbf{q} \cdot \mathbf{m}_w + \frac{c_b}{2}[-H\mathbf{m}_w \cdot \nabla_s(\delta\mathbf{q} \cdot \mathbf{n}) + (\delta\mathbf{q} \cdot \mathbf{n})(\mathbf{m}_w \cdot \nabla_s H) + H^2\delta\mathbf{q} \cdot \mathbf{m}_w]\right)dl, \tag{15}$$

where $[\cdot]_2^1$ denotes the jump across the contact line from Σ_2 to Σ_1.

The governing equations for the static configuration of the system are obtained using the fact that the first variation of $\mathcal{L}$ has to vanish at the equilibrium state. Specifically, on Σ_i ($i = 1, 2$) we have

$$2\gamma_i H - c_b\left(\frac{1}{2}\Delta_s H + H(H^2 - K)\right) - \lambda_i = 0 \quad \text{on } \Sigma_i (i = 1, 2),$$
(16)

where the second term is the bending force resulting from the Willmore free energy, and the Lagrange multipliers λ_i can be interpreted as the pressure in Ω_i. On the droplet surface, we have

$$-2\gamma_3 H + \lambda_2 - \lambda_1 = 0 \quad \text{on } \Sigma_3.$$
(17)

At the contact line Λ, $\delta\mathbf{q}$ and $\nabla_s\delta\mathbf{q}$ are both arbitrary. This yields the following conditions at Λ:

$$\frac{c_b}{2}[H]_2^1 = 0$$
(18)

and

$$\gamma_1\mathbf{m}_1 + \gamma_2\mathbf{m}_2 + \gamma_3\mathbf{m}_3 + \frac{c_b}{2}\mathbf{m}_1 \cdot [\nabla_s H]_2^1\mathbf{n}|_\Xi = \mathbf{0},$$
(19)

where $\mathbf{n}|_\Xi$ denotes the normal vector of the membrane Ξ at the contact line. On the boundary $\partial\Xi$, using the condition $\delta\mathbf{q} \cdot \mathbf{n}_w = 0$ and the fact that both $\delta\mathbf{q}$ and $\nabla_s\delta\mathbf{q}$ are arbitrary, we obtain

$$\frac{c_b}{2}H = 0$$
(20)

and

$$\mathcal{P}_w\left(\gamma_2\mathbf{m}_w + \frac{c_b}{2}(\mathbf{m}_w \cdot \nabla_s H)\mathbf{n}\right) = \mathbf{0},$$
(21)

where $\mathcal{P}_w = \mathbf{I} - \mathbf{n}_w \otimes \mathbf{n}_w$ is the projection operator onto the wall.

Equations (16)–(21) form the governing equations for the static profiles of the membrane and the droplet surface. Note that in the absence of the bending energy, i.e., when $c_b = 0$, the droplet surface and the membrane have constant curvatures and thus assume spherical shapes, and the contact angles satisfy Neumann's law: $\gamma_1\mathbf{m}_1 + \gamma_2\mathbf{m}_2 + \gamma_3\mathbf{m}_3 = 0$.

In the two-dimensional (2D) case, the membrane and the droplet surface are represented by curves. We parametrize the curves as $\mathbf{q}(s)$ and $\mathbf{r}(s)$, respectively. Denote the curvature of the curves by κ: $\kappa = \nabla_s \cdot \mathbf{n}$ on Σ_1 and Σ_2, $\kappa = -\nabla_s \cdot \mathbf{n}$ on Σ_3, where the different signs are due to the fact that the unit normal vector points downward on the membrane and upward on the droplet surface. Then, from the total energy

$$F_2 = \sum_{i=1}^{3}\int_{\Sigma_i}\gamma_i dl + \frac{c_b}{2}\int_\Xi \kappa^2 dl,$$
(22)

we can derive the governing equations for the static profiles of the interfaces following the same procedure as in the above

three-dimensional (3D) case. These equations read

$$\gamma_i\kappa - c_b\left(\Delta_s\kappa + \frac{1}{2}\kappa^3\right) - \lambda_i = 0 \quad \text{on } \Sigma_i \ (i = 1, 2), \quad (23a)$$

$$-\gamma_3\kappa + \lambda_2 - \lambda_1 = 0 \quad \text{on } \Sigma_3, \quad (23b)$$

$$[\kappa]_2^1 = 0,$$

$$\gamma_3\mathbf{m}_3 - (\gamma_2 - \gamma_1)\mathbf{m}_1 + c_b\left(\mathbf{m}_1 \cdot [\nabla_s\kappa]_2^1\right)\mathbf{n}|_\Xi = \mathbf{0} \quad \text{on } \Lambda,$$
(23c)

$$\kappa = 0, \quad \gamma_2\cos\theta_w + c_b(\mathbf{m}_w \cdot \nabla_s\kappa)\sin\theta_w = 0 \quad \text{on } \partial\Xi,$$
(23d)

where $\theta_w \in [0, \pi]$ is the angle measured from the downward tangent vector of the wall to the conormal vector of the membrane $\mathbf{m}_w$, as depicted in Fig. 1.

From the contact line condition (23c), we see that the Young-Dupré equation $\gamma_3\cos\theta_Y = \gamma_2 - \gamma_1$ still holds in the conormal direction of the membrane $\mathbf{m}_1$, where $\theta_Y = \cos^{-1}(\mathbf{m}_3 \cdot \mathbf{m}_1)$ is the contact angle between $\mathbf{m}_3$ and $\mathbf{m}_1$. In addition, we have $\gamma_3\sin\theta_Y = -c_b(\mathbf{m}_1 \cdot [\nabla_s\kappa_i]_2^1)$ in the normal direction $\mathbf{n}$, which states that the surface tension force in the normal direction is balanced by the force resulting from the jump of $\nabla_s\kappa$ across the contact line.

We next analyze the interface profiles based on the governing equations derived above. We first consider the 2D model and study its asymptotic limits when the reduced bending modulus tends to $+\infty$ and 0, respectively. Then we consider the 3D model in the axisymmetric case and show that the asymptotic results derived for the 2D model also hold in three dimensions.

III. ASYMPTOTIC ANALYSIS FOR THE TWO-DIMENSIONAL MODEL

In this section, we perform asymptotic analysis for the 2D model (23a)–(23d). We first make these equations dimensionless by rescaling the variables and parameters as

$$\tilde{s} = s/L, \quad \tilde{\mathbf{q}} = \mathbf{q}/L, \quad \tilde{\mathbf{r}} = \mathbf{r}/L, \quad \tilde{\kappa} = L\kappa,$$

$$\tilde{\gamma}_i = \gamma_i/\gamma_3, \quad \tilde{\lambda}_i = \lambda_i L/\gamma_3, \quad \nu = c_b/(L^2\gamma_3),$$

where we have used the size of the box L as the characteristic length. Then equations (23a)–(23d) become (omitting the overhead tildes)

$$\gamma_i\kappa - \nu\left(\Delta_s\kappa + \frac{1}{2}\kappa^3\right) - \lambda_i = 0 \quad \text{on } \Sigma_i \ (i = 1, 2), \quad (24a)$$

$$-\gamma_3\kappa + \lambda_2 - \lambda_1 = 0 \quad \text{on } \Sigma_3, \quad (24b)$$

$$[\kappa]_2^1 = 0,$$

$$-\gamma_3\mathbf{t}_3 + (\gamma_2 - \gamma_1)\mathbf{t}_1 - \nu\left(\mathbf{t}_1 \cdot [\nabla_s\kappa]_2^1\right)\mathbf{n}|_\Xi = \mathbf{0} \quad \text{on } \Lambda,$$
(24c)

$$\kappa = 0, \quad \gamma_2\cos\theta_w + \nu(\mathbf{t}_2 \cdot \nabla_s\kappa)\sin\theta_w = 0 \quad \text{on } \partial\Xi,$$
(24d)

where we have introduced $\mathbf{t}_i$ ($i = 1, 2, 3$), the unit tangent vectors along the interfaces which point away from the contact line Λ and satisfy $\mathbf{t}_i = -\mathbf{m}_i$ at the contact line.

Next, we consider two limiting cases: (i) $\nu \gg 1$, i.e., $c_b/\gamma_3 \gg L^2$, for a stiff membrane; and (ii) $\nu \ll 1$, i.e., $c_b/\gamma_3 \ll L^2$, for a soft membrane. We will show that in the first case the leading-order solution corresponds to a circular interface on a flat membrane with the contact angle satisfying the conventional Young-Dupré equation; any deviation from this configuration is a regular perturbation effect. In the second case, a two-scale structure emerges near the contact line. The leading-order solution is obtained by matching the interface profiles in the inner and outer regions. In particular, we show that the three apparent contact angles which are defined in the outer region obey Neumann's law.

A. Stiff membrane

We first consider the case where $\nu \gg 1$. Let $\epsilon = \frac{1}{\nu}$ be the small parameter in the problem. We expand the unknown quantities in powers of ϵ as

$$\mathbf{q} = \mathbf{q}_0 + \epsilon \mathbf{q}_1 + \cdots, \quad \mathbf{r} = \mathbf{r}_0 + \epsilon \mathbf{r}_1 + \cdots,$$
$$\lambda_i = \lambda_{i,0} + \epsilon \lambda_{i,1} + \cdots. \tag{25}$$

The tangent and normal vectors, the curvatures, and the surface gradient operator are expanded accordingly as

$$\mathbf{t}_i = \mathbf{t}_{i,0} + \epsilon \mathbf{t}_{i,1} + \cdots, \quad \mathbf{n} = \mathbf{n}_0 + \epsilon \mathbf{n}_1 + \cdots,$$
$$\kappa = \kappa_0 + \epsilon \kappa_1 + \cdots, \quad \nabla_s = \nabla_{s,0} + \epsilon \nabla_{s,1} + \cdots. \tag{26}$$

Substituting these expansions into the above system of equations, we obtain on the leading order $O(1)$ that

$$\Delta_{s,0} \kappa_0 + \tfrac{1}{2} \kappa_0^3 = 0 \quad \text{on } \Sigma_{i,0} \ (i = 1, 2), \tag{27a}$$

$$-\gamma_3 \kappa_0 + \lambda_{2,0} - \lambda_{1,0} = 0 \quad \text{on } \Sigma_{3,0}, \tag{27b}$$

$$[\kappa_0]_2^1 = 0, \quad \mathbf{t}_{1,0} \cdot [\nabla_{s,0} \kappa_0]_2^1 = 0, \quad \text{on } \Lambda_0, \tag{27c}$$

$$\kappa_0 = 0, \quad \mathbf{t}_{2,0} \cdot \nabla_{s,0} \kappa_0 = 0 \quad \text{on } \partial \Xi_0, \tag{27d}$$

where $\Delta_{s,0} = \nabla_{s,0} \cdot \nabla_{s,0}$ is the leading-order Laplace-Beltrami operator.

It is easy to see that a solution is given by

$$\kappa_0 = 0 \quad \text{on } \Sigma_{1,0}, \Sigma_{2,0}; \quad \kappa_0 = \frac{\lambda_{2,0} - \lambda_{1,0}}{\gamma_3} \quad \text{on } \Sigma_{3,0}. \tag{28}$$

This solution corresponds to a flat membrane and a circular droplet surface with a constant curvature which is determined by the two volume constraints. The complete profile of the droplet is yet to be determined, as the contact angle has to be obtained by considering the $O(\epsilon)$ problem.

On the order $O(\epsilon)$, we have

$$\Delta_{s,0} \kappa_1 + \tfrac{1}{2} \kappa_1^3 + \lambda_{i,0} = 0 \quad \text{on } \Sigma_{i,0}, \ (i = 1, 2), \tag{29a}$$

$$-\gamma_3 \kappa_1 + \lambda_{2,1} - \lambda_{1,1} = 0 \quad \text{on } \Sigma_{3,0}, \tag{29b}$$

$$[\kappa_1]_2^1 = 0,$$
$$-\gamma_3 \mathbf{t}_{3,0} + (\gamma_2 - \gamma_1) \mathbf{t}_{1,0} - \big(\mathbf{t}_{1,0} \cdot [\nabla_{s,0} \kappa_1]_2^1 \big) \mathbf{n}_0 \big|_\Xi = \mathbf{0} \quad \text{on } \Lambda_0, \tag{29c}$$

$$\kappa_1 = 0, \quad \gamma_2 \cos \theta_{w,0} + (\mathbf{t}_{2,0} \cdot \nabla_{s,0} \kappa_1) \sin \theta_{w,0} = 0 \quad \text{on } \partial \Xi_0. \tag{29d}$$

From the tangential component of the second equation in (29c), we obtain the Young-Dupré equation for the contact angle:

$$\gamma_3 \cos \theta_{Y,0} = \gamma_2 - \gamma_1, \tag{30}$$

where $\theta_{Y,0} = \cos^{-1}(\mathbf{t}_{3,0} \cdot \mathbf{t}_{1,0})$ is the angle between the leading-order droplet surface and the flat membrane. Together with (30) and the volume constraints, Eq. (28) determines the leading-order profile of the droplet surface.

B. Soft membrane

Next we consider the other limiting case: $\nu \ll 1$ for a soft membrane. In this case, an interior layer appears along the membrane near the contact line. We assume that the size of this inner region is $\xi \ll 1$. We perform the outer and inner expansions separately, then match the two solutions to determine the complete profile of the interfaces.

Outer solution. In the outer region away from the contact line, we use the same expansions as in (25) and (26) but with ϵ replaced by ν. Substituting the expansions into Eqs. (24a), (24b) and (24d), we obtain on the leading order $O(1)$ that

$$\gamma_i \kappa_0 - \lambda_{i,0} = 0 \quad \text{on } \Sigma_{i,0} \ (i = 1, 2), \tag{31a}$$

$$-\gamma_3 \kappa_0 + \lambda_{2,0} - \lambda_{1,0} = 0 \quad \text{on } \Sigma_{3,0}, \tag{31b}$$

$$\kappa_0 = 0, \quad \cos \theta_{w,0} = 0 \quad \text{on } \partial \Xi_0. \tag{31c}$$

This yields the constant-curvature solution

$$\kappa_0 = \frac{\lambda_{1,0}}{\gamma_1} \text{ on } \Sigma_{1,0}; \quad \kappa_0 = \lambda_{2,0} = 0 \text{ on } \Sigma_{2,0};$$
$$\kappa_0 = -\frac{\lambda_{1,0}}{\gamma_3} \text{ on } \Sigma_{3,0}. \tag{32}$$

Together with the boundary condition $\theta_{w,0} = \frac{\pi}{2}$, we obtain that the interface $\Sigma_{2,0}$ in the outer region is part of a horizontal line perpendicular to the vertical wall. The interfaces $\Sigma_{1,0}$ and $\Sigma_{3,0}$ are circular arcs. The configuration is shown in the left panel of Fig. 2.

Also shown in the figure are the angles between the leading-order interfaces in the outer region, denoted by θ_{12}, θ_{23}, and θ_{31} respectively. These are the apparent contact angles, and will be determined by matching with the inner solution.

Inner solution. We focus on the inner region near the left contact line. We rescale the spatial variables by ξ and define the inner variables as

$$\bar{s} = \frac{s - s_l}{\xi}, \quad \bar{\mathbf{q}} = \frac{\mathbf{q} - \mathbf{q}_l}{\xi}, \quad \bar{\mathbf{r}} = \frac{\mathbf{r} - \mathbf{r}_l}{\xi},$$
$$\bar{\kappa} = \xi \kappa, \quad \bar{\lambda}_i = \lambda_i,$$

where $\mathbf{q}_l = \mathbf{r}_l$ is the position of the contact line, and s_l is the parameter value at the contact line. Making the transformations in Eqs. (24a)–(24c) and using dominant balance, we obtain $\xi = \nu^{1/2}$. This states that, near the contact line, the forces due to the surface tension and the bending energy are the dominant terms in the equations.
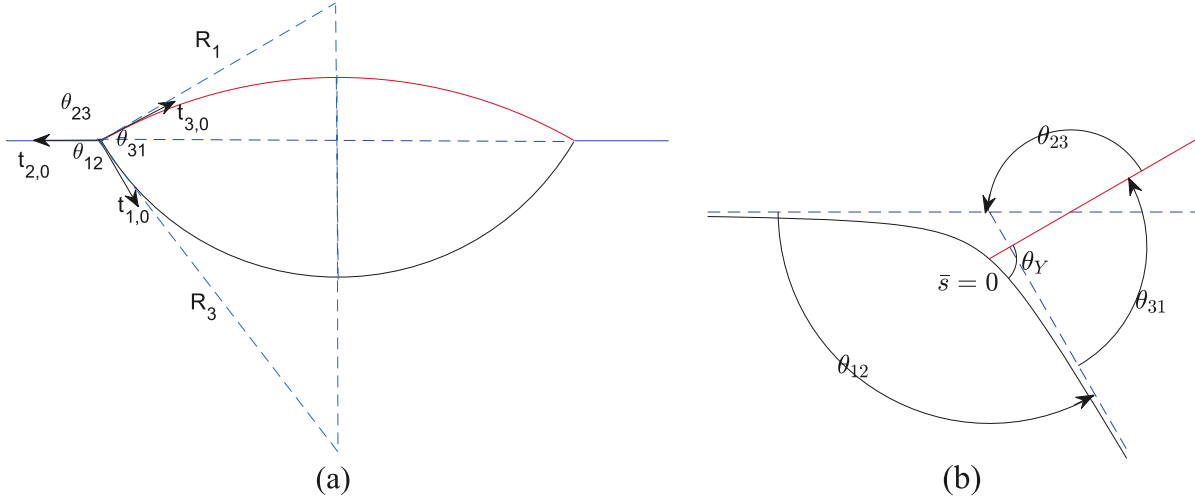
FIG. 2. Sketch of the solutions in the outer (left panel) and inner (right panel) regions. The red and black curves represent the droplet and the membrane surfaces respectively. Left panel: The radii of the leading-order surfaces $\bar{\Sigma}_{1,0}$ and $\bar{\Sigma}_{3,0}$ are given by $R_1 = \frac{\gamma_1}{\lambda_{1,0}}$ and $R_3 = -\frac{\gamma_3}{\lambda_{1,0}}$, respectively. Right panel: The contact point locates at $\bar{s} = 0$, and the apparent contact angles are defined as the angles between the asymptotes of the inner solution as $\bar{s} \to \pm\infty$.

Then we expand the inner variables in ν as

$$\bar{\mathbf{q}} = \bar{\mathbf{q}}_0 + \nu^{1/2}\bar{\mathbf{q}}_1 + \cdots, \quad \bar{\mathbf{r}} = \bar{\mathbf{r}}_0 + \nu^{1/2}\bar{\mathbf{r}}_1 + \cdots,$$

$$\bar{\lambda}_i = \bar{\lambda}_{i,0} + \nu^{1/2}\bar{\lambda}_{i,1} + \cdots. \tag{33}$$

The tangent and normal vectors, the curvature, and the surface gradient operator are expanded accordingly as

$$\bar{\mathbf{t}}_i = \bar{\mathbf{t}}_{i,0} + \nu^{1/2}\bar{\mathbf{t}}_{i,1} + \cdots, \quad \bar{\mathbf{n}} = \bar{\mathbf{n}}_0 + \nu^{1/2}\bar{\mathbf{n}}_1 + \cdots,$$

$$\bar{\kappa} = \bar{\kappa}_0 + \nu^{1/2}\bar{\kappa}_1 + \cdots, \quad \bar{\nabla}_s = \bar{\nabla}_{s,0} + \nu^{1/2}\bar{\nabla}_{s,1} + \cdots, \tag{34}$$

where $\bar{\nabla}_s$ is the surface gradient operator with respect to the rescaled parameter $\bar{s}$.

Using these expansions, we obtain on the leading order $O(1)$ that

$$\gamma_i\bar{\kappa}_0 - \left(\bar{\Delta}_{s,0}\bar{\kappa}_0 + \tfrac{1}{2}\bar{\kappa}_0^3\right) = 0 \quad \text{on } \bar{\Sigma}_{i,0} \ (i = 1, 2), \tag{35a}$$

$$-\gamma_3\bar{\kappa}_0 = 0 \quad \text{on } \bar{\Sigma}_{3,0}, \tag{35b}$$

$$[\bar{\kappa}_0]_2^1 = 0, \tag{}$$

$$-\gamma_3\bar{\mathbf{t}}_{3,0} + (\gamma_2 - \gamma_1)\bar{\mathbf{t}}_{1,0} - \left(\bar{\mathbf{t}}_{1,0} \cdot [\bar{\nabla}_{s,0}\bar{\kappa}_0]_2^1\right)\bar{\mathbf{n}}_0|_\Xi = \mathbf{0} \quad \text{on } \bar{\Lambda}_0. \tag{35c}$$

From (35b), we obtain $\bar{\kappa}_0 = 0$ on $\bar{\Sigma}_{3,0}$. Thus the leading-order profile of the droplet surface is a straight line in the inner region.

To solve (35a), we shall choose the arclength to parametrize the membrane. Under this parametrization, the Laplace-Beltrami operator takes the simple form $\bar{\Delta}_{s,0} = \frac{d^2}{d\bar{s}^2}$. Multiplying both sides of the equation by $\frac{d\bar{\kappa}_0}{d\bar{s}}$ followed by an integration yields

$$\frac{1}{2}\left(\frac{d\bar{\kappa}_0}{d\bar{s}}\right)^2 = -\frac{1}{8}\bar{\kappa}_0^4 + \frac{1}{2}\gamma_i\bar{\kappa}_0^2 + D_i \quad \text{on } \bar{\Sigma}_{i,0} \ (i = 1, 2), \tag{36}$$

where D_1 and D_2 are the integration constants. For the interface, in particular its slope, to asymptotically match between

the inner and outer regions, it is necessary that $\bar{\kappa}_0 \to 0$ and $\frac{d\bar{\kappa}_0}{d\bar{s}} \to 0$ as $\bar{s} \to \pm\infty$. This yields $D_i = 0$ for $i = 1, 2$.

Equation (36) can be further integrated to give

$$\bar{\kappa}_0(\bar{s}) = -\sqrt{4\gamma_i}\,\text{sech}[\sqrt{\gamma_i}(\bar{s} + C_i)] \quad \text{on } \bar{\Sigma}_{i,0} \ (i = 1, 2), \tag{37}$$

where $\text{sech}(x) = \frac{2}{e^x + e^{-x}}$ is the hyperbolic secant function, and C_1 and C_2 are the integration constants. Here we have retained the negative sign based on the observation that $\bar{\kappa}_0(\bar{s}) < 0$ on $\bar{\Sigma}_{i,0} \ (i = 1, 2)$ from the numerical results to be shown in the next section. The constants $C_i \ (i = 1, 2)$ are determined by using the contact line conditions in (35c). Specifically, we have

$$\sqrt{4\gamma_1}\,\text{sech}(\sqrt{\gamma_1}C_1) = \sqrt{4\gamma_2}\,\text{sech}(\sqrt{\gamma_2}C_2) = C, \tag{38a}$$

$$\gamma_3\sin\theta_Y = \sqrt{\gamma_1 C^2 - \frac{1}{4}C^4} + \sqrt{\gamma_2 C^2 - \frac{1}{4}C^4}, \tag{38b}$$

$$\bar{\mathbf{t}}_{3,0} \cdot \bar{\mathbf{t}}_{1,0} = \cos\theta_Y, \tag{38c}$$

where the first equation is from the continuity condition for the curvature, and the last two equations are from the force balance condition in (35c). In Eq. (38c), θ_Y is the Young's angle defined in Eq. (2). Once θ_Y is known, the constants $C > 0$, $C_1 > 0$, and $C_2 < 0$ can be uniquely solved from the algebraic equations (38a) and (38b). Here the sign of $C_i \ (i = 1, 2)$ is chosen based on the observations from the numerical results that $\frac{d\bar{\kappa}_0}{d\bar{s}} > 0$ on $\bar{\Sigma}_{1,0}$ and $\frac{d\bar{\kappa}_0}{d\bar{s}} < 0$ on $\bar{\Sigma}_{2,0}$.

Once C_1 and C_2 have been determined, Eq. (37) can be integrated again to give the interface profile in the inner region. To see this, we let $\bar{\mathbf{t}}_{i,0} = (\cos\bar{\theta}_{i,0}(\bar{s}), \sin\bar{\theta}_{i,0}(\bar{s}))$, where $\bar{\theta}_{i,0}(\bar{s}) \ (i = 1, 2)$ are continuously differentiable and satisfy $\bar{\theta}_{2,0}(0) = \bar{\theta}_{1,0}(0) + \pi$ due to the assumption that the tangent vectors point away from the contact line. Then (37) can be

written as

$$\frac{d\bar{\theta}_{1,0}}{d\bar{s}} = -\sqrt{4\gamma_1}\,\text{sech}[\sqrt{\gamma_1}(\bar{s}+C_1)] \quad \text{for} \quad \bar{s} > 0,$$

(39a)

$$\frac{d\bar{\theta}_{2,0}}{d\bar{s}} = -\sqrt{4\gamma_2}\,\text{sech}[(\sqrt{\gamma_2}(\bar{s}+C_2)] \quad \text{for} \quad \bar{s} < 0.$$

(39b)

Integrating these equations from 0 to $\bar{s}$ respectively yields

$$\bar{\theta}_{1,0}(\bar{s}) = \theta_0 - 2(\tan^{-1}\{\sinh[\sqrt{\gamma_1}(\bar{s}+C_1)]\} - \phi_1),$$
$$\bar{s} > 0,$$

(40a)

$$\bar{\theta}_{2,0}(\bar{s}) = \theta_0 + \pi - 2(\tan^{-1}\{\sinh[\sqrt{\gamma_2}(\bar{s}+C_2)]\} - \phi_2),$$
$$\bar{s} < 0,$$

(40b)

where $\theta_0 = \bar{\theta}_{1,0}(0)$, $\phi_1 = \tan^{-1}[\sinh(\sqrt{\gamma_1}C_1)]$, and $\phi_2 = \tan^{-1}[\sinh(\sqrt{\gamma_2}C_2)]$.

Finally, the constant θ_0 is determined by matching $\bar{\theta}_{2,0}(\bar{s})$ with the outer solution on Σ_2. We have found that the leading-order outer solution for the membrane Σ_2 is a straight line with zero slope, thus $\lim_{\bar{s}\to-\infty}\bar{\theta}_{2,0}(\bar{s}) = \pi$ (mod 2π). This yields

$$\theta_0 = \pi - 2\phi_2.$$

(41)

This completely determines the inner profiles for the interfaces.

Apparent contact angles. The limiting angles of $\bar{\Sigma}_{1,0}$ and $\bar{\Sigma}_{2,0}$ as $\bar{s}\to\pm\infty$ can be readily computed from (40a) and (40b) respectively:

$$\bar{\theta}_{1,0}(+\infty) := \lim_{\bar{s}\to+\infty}\bar{\theta}_{1,0}(\bar{s}) = 2\phi_1 - 2\phi_2,$$

(42a)

$$\bar{\theta}_{2,0}(-\infty) := \lim_{\bar{s}\to-\infty}\bar{\theta}_{2,0}(\bar{s}) = \pi.$$

(42b)

In addition, since the leading-order profile of $\bar{\Sigma}_3$ is a straight line, its angle is a constant and is given by

$$\bar{\theta}_{3,0} = \theta_Y + \theta_0 = \theta_Y + \pi - 2\phi_2.$$

(43)

By the matching condition, these limiting angles agree with the outer solutions (shown in the right panel of Fig. 2). Thus the apparent contact angles defined in the outer region are given by

$$\theta_{12} = \bar{\theta}_{1,0}(+\infty) - \bar{\theta}_{2,0}(-\infty) = 2\phi_1 - 2\phi_2 - \pi,$$

(44a)

$$\theta_{23} = \bar{\theta}_{2,0}(-\infty) - \bar{\theta}_{3,0} = 2\phi_2 - \theta_Y,$$

(44b)

$$\theta_{31} = \bar{\theta}_{3,0} - \bar{\theta}_{1,0}(+\infty) = \pi + \theta_Y - 2\phi_1.$$

(44c)

These angles satisfy Neumann's law,

$$\frac{\sin\theta_{23}}{\gamma_1} = \frac{\sin\theta_{31}}{\gamma_2} = \frac{\sin\theta_{12}}{\gamma_3}.$$

(45)

This can be verified by straightforward algebraic calculations using the trigonometric identities. First,

$$\gamma_2\sin\theta_{12} = -\gamma_2\left(\frac{2\tan\phi_1}{1+\tan^2\phi_1}\frac{1-\tan^2\phi_2}{1+\tan^2\phi_2} - \frac{2\tan\phi_2}{1+\tan^2\phi_2}\frac{1-\tan^2\phi_1}{1+\tan^2\phi_1}\right)$$
$$= -\frac{C^2}{4\gamma_1}[(C^2-2\gamma_2)\tan\phi_1 - (C^2-2\gamma_1)\tan\phi_2],$$

(46)

where we have used the facts that $\tan\phi_1 = \sqrt{4\gamma_1/C^2 - 1}$ and $\tan\phi_2 = -\sqrt{4\gamma_2/C^2 - 1}$ which follow from (38a). Similarly,

$$\gamma_3\sin\theta_{31} = -\left(\frac{C^2}{2}(\tan\phi_1 - \tan\phi_2)\frac{1-\tan^2\phi_1}{1+\tan^2\phi_1} - (\gamma_2-\gamma_1)\frac{2\tan\phi_1}{1+\tan^2\phi_1}\right)$$
$$= -\frac{C^2}{4\gamma_1}[(C^2-2\gamma_2)\tan\phi_1 - (C^2-2\gamma_1)\tan\phi_2],$$

(47)

where we have used the fact that $\gamma_3\sin\theta_Y = \frac{C^2}{2}(\tan\phi_1 - \tan\phi_2)$, which follows from (38b). Therefore, $\gamma_2\sin\theta_{12} = \gamma_3\sin\theta_{31}$. By similar calculations, we can verify that $\gamma_1\sin\theta_{12} = \gamma_3\sin\theta_{23}$. This proves that Neumann's law holds for the three apparent contact angles θ_{12}, θ_{23}, and θ_{31}.

IV. ASYMPTOTIC ANALYSIS FOR THE THREE-DIMENSIONAL AXISYMMETRIC MODEL

The asymptotic results obtained for the 2D model also hold for 3D systems. We consider the axisymmetric case for ease of presentation. Using the dimensionless variables and parameters as defined in the 2D model, the dimensionless model in 3D reads

$$2\gamma_i H - \nu\left(\frac{1}{2}\Delta_s H + H(H^2-K)\right) - \lambda_i = 0 \quad \text{on } \Sigma_i(i=1,2),$$

(48a)

$$-2\gamma_3 H + \lambda_2 - \lambda_1 = 0 \quad \text{on } \Sigma_3,$$

(48b)

$$[H]_2^1 = 0,$$

$$\gamma_3\boldsymbol{m}_3 - (\gamma_2-\gamma_1)\boldsymbol{m}_1 + \frac{\nu}{2}(\boldsymbol{m}_1\cdot[\nabla_s H]_2^1)\boldsymbol{n}|_\Xi = \boldsymbol{0} \quad \text{on } \Lambda,$$

(48c)

$$H = 0, \quad \gamma_2\cos\theta_w + \frac{\nu}{2}(\boldsymbol{m}_w\cdot\nabla_s H)\sin\theta_w = 0 \quad \text{on } \partial\Xi.$$

(48d)

Since the membrane and the droplet are axisymmetric and can be generated by the curve $(r(s), z(s))$ revolving about the symmetry axis, they can be parametrized in the form $(r(s)\cos\theta, r(s)\sin\theta, z(s))$ where $s\in R$ and $\theta\in[0, 2\pi]$ are

parameters. In this parametrization, the contravariant basis and the covariant basis are given by

$$\mathbf{t}_s = (r' \cos \theta, r' \sin \theta, z'), \quad \mathbf{t}_\theta = (-r \sin \theta, r \cos \theta, 0),$$

$$\mathbf{t}^s = \frac{1}{r'^2 + z'^2}(r' \cos \theta, r' \sin \theta, z'),$$

$$\mathbf{t}^\theta = \left(-\frac{1}{r} \sin \theta, \frac{1}{r} \cos \theta, 0\right).$$

The mean curvature and the Gaussian curvature are given by

$$H = \tfrac{1}{2}(\kappa_r + \kappa_\theta), \quad K = \kappa_r \kappa_\theta, \tag{49}$$

where κ_r and κ_θ are the two principal curvatures given by

$$\kappa_r = \frac{r'z'' - r''z'}{(r'^2 + z'^2)^{3/2}}, \tag{50a}$$

$$\kappa_\theta = \frac{z'}{r(r'^2 + z'^2)^{1/2}}. \tag{50b}$$

The surface gradient and Laplacian operators are given by

$$\nabla_s = \mathbf{t}^s \frac{\partial}{\partial s} + \mathbf{t}^\theta \frac{\partial}{\partial \theta}, \tag{51a}$$

$$\Delta_s = \frac{1}{r'^2 + z'^2} \frac{\partial^2}{\partial s^2} - \frac{r'r'' + z'z''}{(r'^2 + z'^2)^2} \frac{\partial}{\partial s}$$

$$+ \frac{r'}{r(r'^2 + z'^2)} \frac{\partial}{\partial s} + \frac{1}{r^2} \frac{\partial^2}{\partial \theta^2}. \tag{51b}$$

Now we consider asymptotic results of the system in the stiff limit and the soft limit, respectively. In the case of a stiff membrane with $\nu \gg 1$, an analysis similar to that in the 2D case gives the leading order solution, which corresponds to a planar membrane and a spherical cap configuration for the droplet with the contact angle satisfying the Young-Dupré equation.

In the case of a soft membrane, $\nu \ll 1$, the outer solution is the same as that in 2D and corresponds to spherical shapes for Σ_1 and Σ_3 and a planar surface perpendicular to the vertical wall for Σ_2. To find the inner solution, we rescale the spatial variables by $\nu^{1/2}$ and define the inner variables as

$$\bar{s} = \frac{s - s_l}{\nu^{1/2}}, \quad \bar{r} = \frac{r - r_l}{\nu^{1/2}}, \quad \bar{z} = \frac{z - z_l}{\nu^{1/2}},$$

where s_l, r_l, z_l are values of s, r, and z at the contact line, respectively. The mean and Gaussian curvatures transform to

$$H = \tfrac{1}{2}(\nu^{-1/2}\bar{\kappa}_r + \bar{\kappa}_\theta), \quad K = \nu^{-1/2}\bar{\kappa}_r\bar{\kappa}_\theta, \tag{52}$$

where $\bar{\kappa}_r$ and $\bar{\kappa}_\theta$ are given by

$$\bar{\kappa}_r = \frac{\bar{r}'\bar{z}'' - \bar{r}''\bar{z}'}{(\bar{r}'^2 + \bar{z}'^2)^{3/2}}, \tag{53a}$$

$$\bar{\kappa}_\theta = \frac{\bar{z}'}{(\nu^{1/2}\bar{r} + r_l)(\bar{r}'^2 + \bar{z}'^2)^{1/2}}. \tag{53b}$$

The surface gradient and surface Laplacian transform to

$$\nabla_s = \nu^{-1/2}\bar{\nabla}_s^a + \bar{\nabla}_s^b, \tag{54a}$$

$$\Delta_s = \nu^{-1}\bar{\Delta}_s^a + \nu^{-1/2}\bar{\Delta}_s^b + \bar{\Delta}_s^c, \tag{54b}$$

where

$$\bar{\nabla}_s^a = \frac{1}{\bar{r}'^2 + \bar{z}'^2}(\bar{r}' \cos \theta, \bar{r}' \sin \theta, \bar{z}') \frac{\partial}{\partial \bar{s}},$$

$$\bar{\nabla}_s^b = \frac{1}{\nu^{1/2}\bar{r} + r_l}(-\sin \theta, \cos \theta, 0) \frac{\partial}{\partial \theta},$$

$$\bar{\Delta}_s^a = \frac{1}{\bar{r}'^2 + \bar{z}'^2} \frac{\partial^2}{\partial \bar{s}^2} - \frac{\bar{r}'\bar{r}'' + \bar{z}'\bar{z}''}{(\bar{r}'^2 + \bar{z}'^2)^2} \frac{\partial}{\partial \bar{s}},$$

$$\bar{\Delta}_s^b = \frac{\bar{r}'}{(\nu^{1/2}\bar{r} + r_l)(\bar{r}'^2 + \bar{z}'^2)} \frac{\partial}{\partial \bar{s}},$$

$$\bar{\Delta}_s^c = \frac{1}{(\nu^{1/2}\bar{r} + r_l)^2} \frac{\partial^2}{\partial \theta^2}.$$

Making these transformations in Eqs. (48a)–(48d), we obtain the leading-order problem

$$4\gamma_i \bar{\kappa}_{r,0} - \left(\bar{\Delta}_{s,0}^a \bar{\kappa}_{r,0} + \tfrac{1}{2}\bar{\kappa}_{r,0}^3\right) = 0 \quad \text{on } \bar{\Sigma}_{i,0}(i = 1, 2), \tag{55a}$$

$$\bar{\kappa}_{r,0} = 0 \quad \text{on } \bar{\Sigma}_{3,0}, \tag{55b}$$

$$[\bar{\kappa}_{r,0}]_2^1 = 0,$$

$$4\gamma_3 \bar{\mathbf{m}}_{3,0} - 4(\gamma_2 - \gamma_1)\bar{\mathbf{m}}_{1,0}$$

$$+ \left(\bar{\mathbf{m}}_{1,0} \cdot \left[\bar{\nabla}_{s,0}^a \bar{\kappa}_{r,0}\right]_2^1\right) \bar{\mathbf{n}}_0|_\Xi = \mathbf{0} \quad \text{on } \bar{\Lambda}_0. \tag{55c}$$

We notice that $\bar{\kappa}_{r,0}$ is the curvature of the generating curve and $\bar{\Delta}_{s,0}^a$ is the surface Laplacian along the curve. Therefore, this leading-order inner problem is the same as the 2D problem (35a)–(35c), after replacing $4\gamma_i$ by γ_i. Thus, we have the same inner solution as in the 2D problem. Together with the same outer solutions, the asymptotic results obtained for the 2D problem also hold for the 3D problem. In particular, the three apparent contact angles obey Neumann's law.

V. NUMERICAL SOLUTIONS

In this section, we solve Eqs. (24a)–(24d) numerically by means of gradient flow. The membrane $\Xi = \Sigma_1 \cup \Sigma_2 \cup \Lambda$ evolves according to the normal velocity given by

$$v_n = -\gamma\kappa + \nu\left(\Delta_s\kappa + \tfrac{1}{2}\kappa^3\right) + \lambda - \gamma_3 \sin\theta_d \delta(s - s_l), \tag{56}$$

with the boundary condition (24d). Here, γ and λ are piecewise constant functions: $\gamma = \gamma_1\chi_1 + \gamma_2\chi_2$, $\lambda = \lambda_1\chi_1 + \lambda_2\chi_2$, with χ_i being the characteristic function on Σ_i ($i = 1, 2$); $\delta(s - s_l)$ is the Dirac delta function concentrated at the contact line, and $\theta_d = \cos^{-1}(\mathbf{t}_1 \cdot \mathbf{t}_3)$ is the dynamic contact angle between the droplet surface and the membrane. The contact line moves along the membrane with the velocity

$$v_l = \gamma_3(\cos\theta_d - \cos\theta_Y)\mathbf{t}_1, \tag{57}$$

where θ_Y is the static contact angle determined by the Young-Dupré equation. In addition, the droplet is assumed to relax infinitely fast, so (24b) is satisfied at any instant. The droplet surface has a circular profile which can be uniquely determined by the contact line location and the volume constraint.

It can be easily seen that, at the steady state when $v_n = v_l = 0$, the solution satisfies the governing equations (24a)–(24d). In particular, an integration of (56) over a control volume with infinitesimal thickness across the contact line yields

$$-\gamma_3 \sin \theta_d + v[\nabla_s \kappa]_2^1 \cdot \mathbf{t}_1 = 0, \tag{58}$$

which is the normal component of (24c) (the second equation). Equation (57) with $v_l = 0$ is equivalent to the tangential component of (24c) (the second equation).

A. Numerical methods

We parametrize the membrane as $(x, y(x, t))$, where $x \in D_m = [-1, 1]$. The two contact points are located at $(x_l^i, y(x_l^i, t))$, with the dynamic contact angles θ_d^i ($i = 1, 2$). Under this parametrization, the dynamic equations (56)–(57) can be written as (up to a constant shift of the solution)

$$\frac{\partial y}{\partial t} = \frac{1}{c}\gamma\kappa - v\left(c\frac{\partial^2\kappa}{\partial x^2} - c^3\frac{\partial y}{\partial x}\frac{\partial^2 y}{\partial x^2}\frac{\partial\kappa}{\partial x} + \frac{1}{2c}\kappa^3\right)$$

$$+ \gamma_3 \sum_{i=1}^{2} \sin\theta_d^i \delta(x - x_l^i) - \frac{1}{c}\xi, \quad x \in D_m \tag{59}$$

$$\frac{dx_l^i}{dt} = \gamma_3\left(\cos\theta_d^i - \cos\theta_Y\right)\cdot c|_{x=x_l^i}, \quad i = 1, 2 \tag{60}$$

with

$$\kappa = c^3\frac{\partial^2 y}{\partial x^2}, \quad x \in D_m \tag{61}$$

and the boundary conditions

$$\kappa = 0, \quad \gamma_2\frac{\partial y}{\partial x} - cv\frac{\partial\kappa}{\partial x} = 0 \quad \text{for } x = \pm 1. \tag{62}$$

Here, $c = 1/\sqrt{1 + (\frac{\partial y}{\partial x})^2}$, and

$$\gamma(x, t) = \gamma_1\chi_{(x_l^1, x_l^2)}(x) + \gamma_2\chi_{D_m\setminus(x_l^1, x_l^2)}(x),$$

$$\xi(x, t) = (\lambda_1 - \lambda_2)\chi_{(x_l^1, x_l^2)}(x) = \frac{\gamma_3}{R}\chi_{(x_l^1, x_l^2)}(x),$$

where R is the radius of curvature of the droplet. The second equality of the above equation follows from the assumption that the droplet is at equilibrium at all times. Note that we need to shift the solution $y = y(x, t)$ to meet the area constraint of Ω_2.

We use a semi-implicit finite difference scheme to solve the above system of equations. The spatial-temporal domain is discretized using a uniform mesh with $-1 = x_0 < x_1 < \cdots < x_n = 1$ and $0 = t_0 < t_1 < \cdots < t_m < \cdots$,
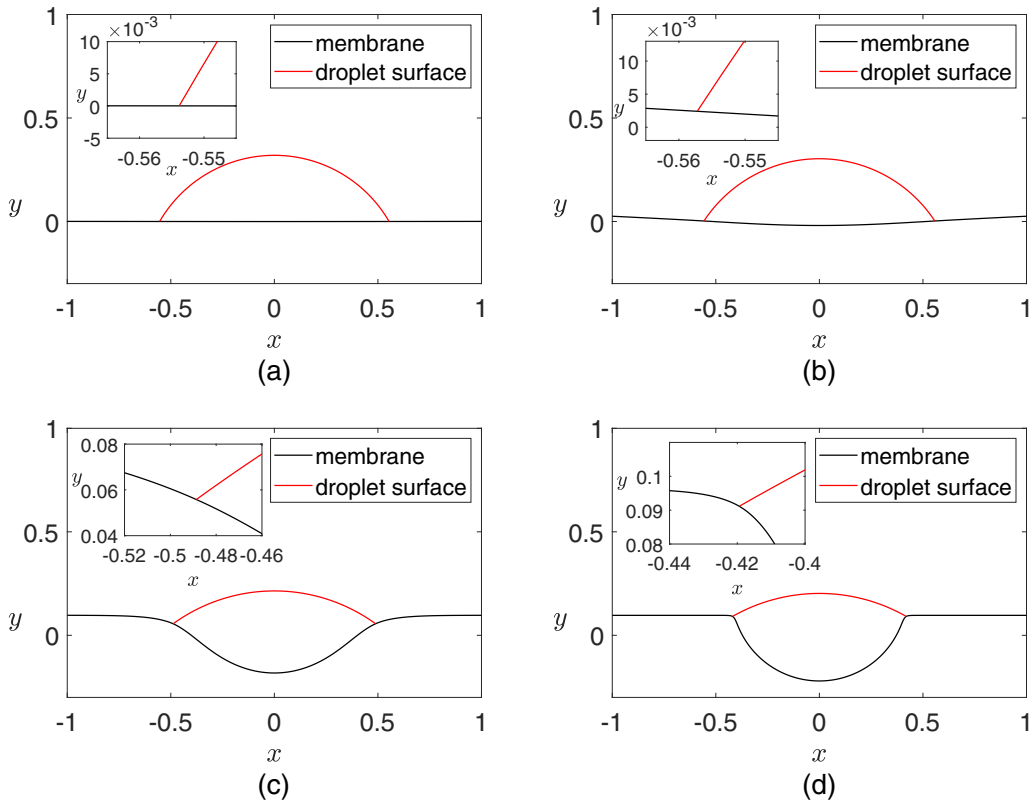

FIG. 3. Interface profiles for the hydrophilic case with $\theta_Y = \pi/3$ and different values of v: $v = 100$ (upper left), $v = 1$ (upper right), $v = 10^{-2}$ (lower left), and $v = 10^{-4}$ (lower right). The insets show the interface profiles near the contact line where the contact angle $\theta_Y = \pi/3$ can be observed.

where $x_{j+1} - x_j = h = 2/n$ and $t_{m+1} - t_m = \Delta t$. Denote by y_j^m, κ_j^m, $x_{l,i}^m$ and $\theta_{d,i}^m$ $(i = 1, 2)$ the numerical approximations to $y(x_j, t_m)$, $\kappa(x_j, t_m)$, $x_l^i(t_m)$, $\theta_d^i(t_m)$, respectively. The finite-difference discretization of (59)–(62) reads

$$\frac{y_j^{m+1} - y_j^m}{\Delta t} = \frac{1}{c_j^m} \gamma_j^m \kappa_j^{m+1} - \nu \left(c_j^m D_x^2 \kappa_j^{m+1} - \left(c_j^m \right)^3 D_x y_j^m D_x^2 y_j^m D_x \kappa_j^{m+1} + \frac{1}{2c_j^m} \left(\kappa_j^m \right)^2 \kappa_j^{m+1} \right)$$

$$+ \gamma_3 \sum_{i=1}^{2} \sin \theta_{d,i}^m \delta_h \left(x_j - x_{l,i}^m \right) - \frac{1}{c_j^m} \xi_j^m, \quad j = 0, 1, \ldots, n, \tag{63a}$$

$$\frac{x_{l,i}^{m+1} - x_{l,i}^m}{\Delta t} = \gamma_3 \left(\cos \theta_{d,i}^m - \cos \theta_Y \right) \cdot c|_{x = x_{l,i}^m}, \quad i = 1, 2 \tag{63b}$$

$$\kappa_j^{m+1} = \left(c_j^m \right)^3 D_x^2 y_j^{m+1}, \quad j = 0, 1, \ldots, n \tag{63c}$$

$$\kappa_j^{m+1} = 0, \quad \gamma_2 D_x y_j^{m+1} - c_j^m \nu D_x \kappa_j^{m+1} = 0, \quad j = 0, n, \tag{63d}$$

where $m = 0, 1, \ldots$, $\gamma_j^m = \gamma(x_j, t_m)$, $\xi_j^m = \xi(x_j, t_m)$, $c_j^m = 1/\sqrt{1 + (D_x y_j^m)^2}$, D_x and D_x^2 are the standard centered finite difference operators,

$$D_x y_j = \frac{y_{j+1} - y_{j-1}}{2h}, \quad D_x^2 y_j = \frac{y_{j+1} - 2y_j + y_{j-1}}{h^2},$$

and similarly for $D_x \kappa_j$ and $D_x^2 \kappa_j$. The Dirac delta function and the characteristic functions are smoothed out to the neighboring grid points.

Equations (63a), (63c), and (63d) form a linear system for $\{y_j^{m+1}, \kappa_j^{m+1} : j = -1, 0, \ldots, n+1\}$. This system is solved at each time step, followed by a shift of the interface $\{y_j^{m+1}\}$ to satisfy the area constraint of Ω_2. The updating procedure is summarized as follows: Given $\{y_j^m, \kappa_j^m : j = -1, 0, \ldots, n+1\}$ and $\{x_{l,i}^m : i = 1, 2\}$,

(1) Use the area constraint for Ω_1 to determine the droplet configuration, in particular, its contact angles $\theta_{d,i}^m$ $(i = 1, 2)$.

(2) Solve the linear system (63a), (63c), and (63d) for $\{y_j^{m+1}, \kappa_j^{m+1} : j = -1, 0, \ldots, n+1\}$.

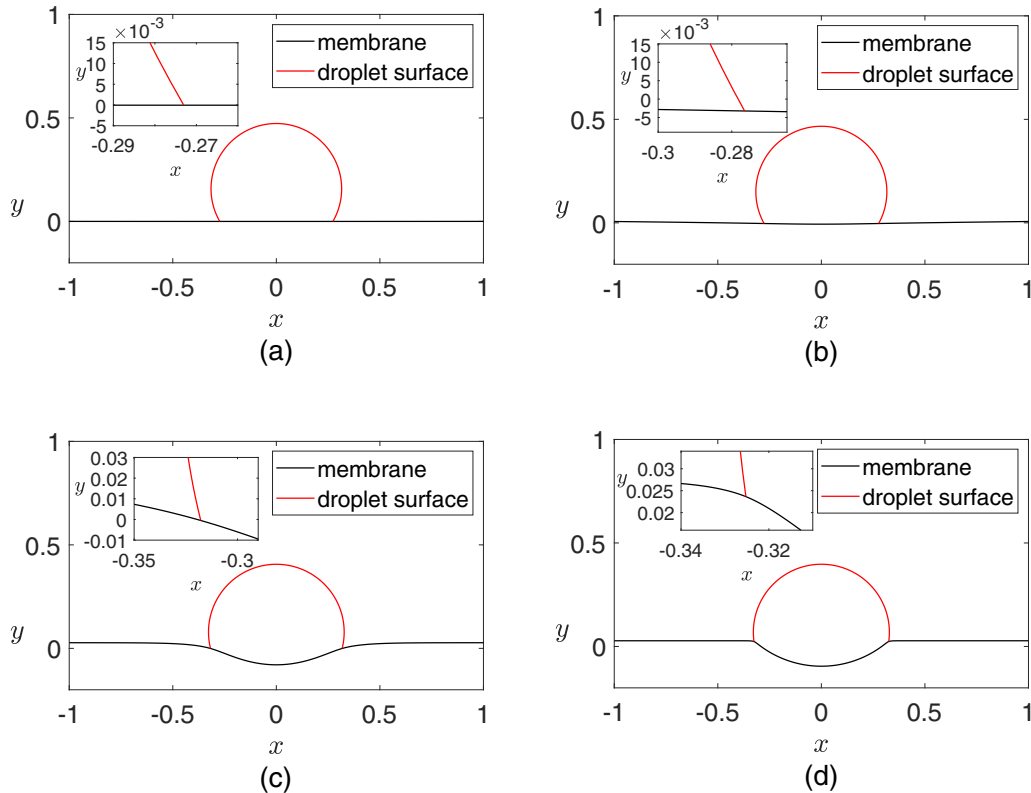(3) Update the contact line position $\{x_{l,i}^{m+1} : i = 1, 2\}$ according to (63b).

FIG. 4. Interface profiles for the hydrophobic case with $\theta_Y = 2\pi/3$ and different values of ν: $\nu = 100$ (upper left), $\nu = 1$ (upper right), $\nu = 10^{-2}$ (lower left), and $\nu = 10^{-4}$ (lower right). The insets show the interface profiles near the contact line where the contact angle $\theta_Y = 2\pi/3$ can be observed.

The computation is terminated when the steady state is reached. In practice, we terminate the computation when $\max_{0 \leqslant j \leqslant n} |y_j^{m+1} - y_j^m| < \text{tol}$ for some small tolerance tol.

B. Numerical results

We consider two examples: one a hydrophilic case with the static contact angles $\theta_Y = \pi/3$ and the other a hydrophobic case with $\theta_Y = 2\pi/3$. The surface tension coefficients are $\gamma_1 = 0.5$, $\gamma_2 = \gamma_3 = 1$ for the hydrophilic case and $\gamma_1 = 1.5$, $\gamma_2 = \gamma_3 = 1$ for the hydrophobic case. Initially, the membrane is flat and the droplet is given by a semicircle with radius $R = 0.4$. The reduced bending modulus of the membrane varies between $\nu = 100$ and $\nu \approx 10^{-6}$. The mesh size h ranges from 10^{-2} for $\nu = 100$ to $\frac{10}{3} \times 10^{-4}$ for $\nu \approx 10^{-6}$. The time step Δt ranges from 10^{-2} for $\nu = 100$ to 10^{-4} for $\nu \approx 10^{-6}$.

The numerical results for the interface profiles are shown in Fig. 3 for the hydrophilic case and Fig. 4 for the hydrophobic case. The different panels in the figures correspond to different values of ν. It is seen that the membrane is stiff and does not deform much when ν is the large (upper panels); in contrast,

TABLE I. The apparent contact angles computed from the numerical solutions for the hydrophilic case (top) and hydrophobic case (bottom). These values agree well with the theoretical values predicted by Neumann's law ($\nu = 0$).

ν	θ_{12}	θ_{23}	θ_{31}
1×10^{-4}	2.4204	1.4322	2.4305
$\frac{1}{4} \times 10^{-4}$	2.4196	1.4389	2.4247
$\frac{1}{16} \times 10^{-4}$	2.4196	1.4413	2.4223
$\frac{1}{64} \times 10^{-4}$	2.4192	1.4429	2.4211
0	2.4189	1.4455	2.4189
1×10^{-4}	1.7049	2.6234	1.9549
$\frac{1}{4} \times 10^{-4}$	1.7753	2.6299	1.8780
$\frac{1}{16} \times 10^{-4}$	1.8088	2.6342	1.8402
$\frac{1}{64} \times 10^{-4}$	1.8287	2.6370	1.8175
0	1.8235	2.6362	1.8235

it becomes rather soft and large deformation occurs when ν is small (lower panels). In both cases, the microscopic contact angle is independent of ν and remains $\pi/3$ and $2\pi/3$ when ν varies from 100 to 10^{-4}, respectively. This can be observed from the insets of the figures.

In Fig. 5, we plot the angle of the membrane for small values of ν ranging from 10^{-4} to 10^{-6}. From the numerical results (insets), we clearly observe the existence of a transition layer near the contact line, whose width decreases with ν. After rescaling the s coordinate by $\sqrt{\nu}$, these solutions agree well with the solution obtained from the asymptotic analysis [(40a) and (40b)]. The agreement improves as the value of ν decreases.

The apparent contact angles for the solutions shown in Fig. 5 are presented in Table I. These angles are computed by reconstructing the membrane and the droplet using their curvatures obtained in the numerical solution away from the contact line (the outer region). These values are compared with the theoretical values predicted by Neumann's law ($\nu = 0$). They agree well in the small bending modulus limit. This again validates the results obtained from the asymptotic analysis.

VI. CONCLUSION

We have considered contact lines on an elastic membrane and studied the static profiles of the interfaces. Such systems arise, for example, when a vesicle is in contact with an interface between two fluids. This work also sheds light on other systems involving deformable substrates, e.g., in coating and the design of smart surfaces.

We derived the governing equations for the static problem by minimizing the total energy, which consisted of the surface energies and the bending energy of the membrane. In this model, the membrane is locally flat at the contact line due to the regularization effect of the Willmore energy. The contact angle satisfies the Young-Dupré equation, which describes the force balance along the membrane. The gradient of the mean curvature of the membrane, however, exhibits a jump across the contact line, which produces a balancing force for the surface tension in the normal direction of the membrane.
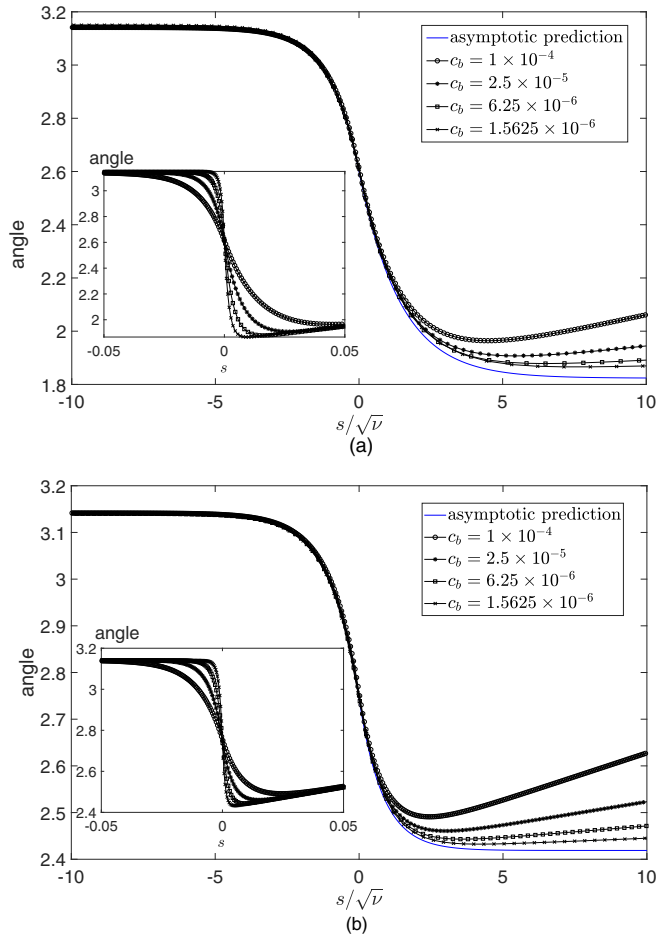

FIG. 5. The angle of the membrane for small values of ν in the hydrophilic case (upper panel) and hydrophobic case (lower panel). The contact line is shifted to $s = 0$ and the s coordinate is rescaled by $\sqrt{\nu}$. The asymptotic solution in (40b) is shifted by π so that the angle is continuous at the contact line. Insets: numerical solutions for the angle before rescaling.

We carried out asymptotic analysis for the model in the limits as the reduced bending modulus ν tends to $+\infty$ and 0, respectively. Asymptotic solutions in both cases were obtained. We found that, in the stiff limit, the leading-order profiles of the interfaces are those of a circular droplet sitting on a rigid substrate with the contact angle satisfying the Young-Dupré equation. In the soft limit, a transition layer with width $\nu^{1/2}$ appears near the contact line, and we computed the leading-order solutions in the inner and outer regions using the matched asymptotic technique. The leading-order interfaces in the outer region have constant curvatures, and the apparent contact angles between them obey Neumann's law.

We also developed an efficient numerical method to compute the static profiles of the interfaces. The numerical method is based on the gradient flow and semi-implicit finite difference discretization. We simulated two systems, one in the hydrophilic case and the other in the hydrophobic case. The numerical results agreed very well with the asymptotic solutions.

In the current work, we only considered the bending energy of the membrane, and neglected the stretching energy. As a result, the problem only involved the geometry of the interfaces. The stretching energy penalizes the extension/contraction of the membrane. In earlier work, a local inextensibility condition has been used to prohibit the extension/contraction of the membrane [16–18], and this models systems with very large stretching energy. In the general situation, one needs to take the strain into account in order to model the stretching energy. We will investigate the effect of the stretching energy on the interface profiles in the future work.

In future work, we also intend to study the dynamical problem which couples the evolution of interfaces and contact lines with hydrodynamics. This extends the classical moving contact line problem, for which most of the earlier work has focused on rigid substrates [29–38]. The dynamical problem is more challenging as one has to couple the dynamics of the substrate, the evolution of the fluid interface, and the motion of the contact line with hydrodynamics equations; in particular, one has to deal with the difficulty arising from the inconsistency of the classical no-slip boundary condition with the contact line motion. We will leave these issues to our future work.

APPENDIX A: VARIATION OF VOLUMES AND SURFACE AREAS

Let $\mathbf{x} = (x_1, x_2, x_3)$ and $\mathbf{X} = (X_1, X_2, X_3)$ denote the Eulerian and Lagrangian coordinates of a fluid parcel, respectively, and $\mathbf{q}(s^1, s^2)$ denote a surface parametrized by (s^1, s^2). Furthermore, let $\mathcal{D}$ be a differential or variation operator which satisfies the chain rule and product rule, and commutes with the spatial differential operator.

For the volume element $\det\left(\frac{\partial \mathbf{x}}{\partial \mathbf{X}}\right)$, we have

$$\mathcal{D}\det\left(\frac{\partial \mathbf{x}}{\partial \mathbf{X}}\right) = \sum_{\sigma \in S_3} \text{sgn}(\sigma)\left(\frac{\partial \mathcal{D}x_1}{\partial X_{\sigma_1}}\frac{\partial x_2}{\partial X_{\sigma_2}}\frac{\partial x_3}{\partial X_{\sigma_3}} + \frac{\partial x_1}{\partial X_{\sigma_1}}\frac{\partial \mathcal{D}x_2}{\partial X_{\sigma_2}}\frac{\partial x_3}{\partial X_{\sigma_3}} + \frac{\partial x_1}{\partial X_{\sigma_1}}\frac{\partial x_2}{\partial X_{\sigma_2}}\frac{\partial \mathcal{D}x_3}{\partial X_{\sigma_3}}\right) = (\nabla \cdot \mathcal{D}\mathbf{x})\det\left(\frac{\partial \mathbf{x}}{\partial \mathbf{X}}\right), \quad \text{(A1)}$$

where $\sigma = (\sigma_i)_{i=1}^3$ is a permutation in the symmetric group S_3 and ∇ is the gradient operator with respect to $\mathbf{x}$. In the second equality, we have used the chain rule $\frac{\partial \mathcal{D}x_i}{\partial X_{\sigma_i}} = \sum_{k=1}^3 \frac{\partial \mathcal{D}x_i}{\partial x_k}\frac{\partial x_k}{\partial X_{\sigma_i}}$.

For the surface element $\sqrt{h} = |\frac{\partial \mathbf{q}}{\partial s^1} \times \frac{\partial \mathbf{q}}{\partial s^2}|$, we have

$$\mathcal{D}\sqrt{h} = \frac{1}{\sqrt{h}}\left(\frac{\partial \mathbf{q}}{\partial s^1} \times \frac{\partial \mathbf{q}}{\partial s^2}\right) \cdot \left(\frac{\partial \mathcal{D}\mathbf{q}}{\partial s^1} \times \frac{\partial \mathbf{q}}{\partial s^2} + \frac{\partial \mathbf{q}}{\partial s^1} \times \frac{\partial \mathcal{D}\mathbf{q}}{\partial s^2}\right) = \sqrt{h}\left(\mathbf{t}^1 \cdot \frac{\partial \mathcal{D}\mathbf{q}}{\partial s^1} + \mathbf{t}^2 \cdot \frac{\partial \mathcal{D}\mathbf{q}}{\partial s^2}\right) = \sqrt{h}(\nabla_s \cdot \mathcal{D}\mathbf{q}), \quad \text{(A2)}$$

where $\{\mathbf{t}^1, \mathbf{t}^2\}$ is the covariate basis of the tangent plane to the surface and ∇_s is the surface gradient operator.

Now we consider two special choices of $\mathcal{D}$. First, if $\mathcal{D} = \frac{\partial}{\partial t}$, we obtain

$$\frac{\partial}{\partial t}\det\left(\frac{\partial \mathbf{x}}{\partial \mathbf{X}}\right) = (\nabla \cdot \dot{\mathbf{x}})\det\left(\frac{\partial \mathbf{x}}{\partial \mathbf{X}}\right), \quad \text{(A3)}$$

$$\frac{\partial}{\partial t}\sqrt{h} = (\nabla_s \cdot \dot{\mathbf{q}})\sqrt{h}, \quad \text{(A4)}$$

where the overhead dot denotes the derivative with respect to t. It follows that, for a given function f defined in a 3D domain Ω and a surface Σ, respectively,

$$\frac{d}{dt}\int_\Omega f(\mathbf{x}, t)d\mathbf{x} = \int_\Omega \left(\frac{\partial f}{\partial t} + \mathbf{u} \cdot \nabla f + (\nabla \cdot \mathbf{u})f\right)d\mathbf{x}, \quad \text{(A5)}$$

$$\frac{d}{dt}\int_\Sigma f(\mathbf{q}, t)dA = \int_\Sigma \left(\frac{\partial f}{\partial t} + \mathbf{u} \cdot \nabla f + (\nabla_s \cdot \mathbf{u})f\right)dA. \quad \text{(A6)}$$

where $\mathbf{u} = \dot{\mathbf{x}}$ in (A5) and $\mathbf{u} = \dot{\mathbf{q}}$ in (A6).

Next, we take the variation operator $\mathcal{D} = \delta$ in (A1) and (A2). We obtain

$$\delta \det \left(\frac{\partial \mathbf{x}}{\partial \mathbf{X}} \right) = (\nabla \cdot \delta \mathbf{x}) \det \left(\frac{\partial \mathbf{x}}{\partial \mathbf{X}} \right), \qquad (A7)$$

$$\delta \sqrt{h} = (\nabla_s \cdot \delta \mathbf{q}) \sqrt{h}. \qquad (A8)$$

It follows that

$$\delta \int_\Omega d\mathbf{x} = \int_\Omega (\nabla \cdot \delta \mathbf{x}) d\mathbf{x} = \int_{\partial \Omega} \mathbf{n} \cdot \delta \mathbf{x} dA, \qquad (A9)$$

$$\delta \int_\Sigma dA = \int_\Sigma (\nabla_s \cdot \delta \mathbf{q}) dA = \int_{\partial \Sigma} \delta \mathbf{q} \cdot \mathbf{m} dl$$
$$- \int_\Sigma \delta \mathbf{q} \cdot (2H\mathbf{n}) dA, \qquad (A10)$$

where $\mathbf{n}$ is the outward normal of $\partial \Omega$ in (A9) and $H = -\frac{1}{2} \nabla_s \cdot \mathbf{n}$ with $\mathbf{n}$ being the normal to Σ whose direction is such that H is positive when the surface curves towards $\mathbf{n}$ in (A10); $\mathbf{m}$ is the outward conormal to $\partial \Sigma$. In (A10), we have used the surface divergent theorem [39].

APPENDIX B: VARIATION OF THE WILLMORE ENERGY

For a surface $\mathbf{x} = \mathbf{q}(s^1, s^2)$, the contravariant basis vectors of the tangent plane of the surface are given by $\mathbf{t}_i = \frac{\partial \mathbf{q}}{\partial s^i}$ ($i = 1, 2$). The first fundamental form is

$$I = h_{11} ds^1 ds^1 + 2h_{12} ds^1 ds^2 + h_{22} ds^2 ds^2, \qquad (B1)$$

where $h_{ij} = \mathbf{t}_i \cdot \mathbf{t}_j$ ($i, j = 1, 2$). Define the symmetric metric tensor

$$M_I = \begin{pmatrix} h_{11} & h_{12} \\ h_{12} & h_{22} \end{pmatrix}, \qquad (B2)$$

and denote its determinant by $h = h_{11}h_{22} - h_{12}^2 = |\mathbf{t}_1 \times \mathbf{t}_2|^2$. The unit normal vector to the surface is given by $\mathbf{n} = \frac{1}{\sqrt{h}} \mathbf{t}_1 \times \mathbf{t}_2$. The covariant basis $\{\mathbf{t}^1, \mathbf{t}^2\}$ of the tangent plane is defined as the reciprocal basis set satisfying $\mathbf{t}^i \cdot \mathbf{t}_j = \delta^i_j$, where δ^i_j is the Kronecker delta. It is easy to see that $h^{ij} = \mathbf{t}^i \cdot \mathbf{t}^j$ is the (i, j)th entry of M_I^{-1}, and $\mathbf{t}^i = h^{im} \mathbf{t}_m$, where we have used the Einstein summation convention.

The second fundamental form is given by

$$II = l_{11} ds^1 ds^1 + 2l_{12} ds^1 ds^2 + l_{22} ds^2 ds^2, \qquad (B3)$$

where $l_{ij} = \frac{\partial \mathbf{t}_i}{\partial s^j} \cdot \mathbf{n} = -\mathbf{t}_i \cdot \frac{\partial \mathbf{n}}{\partial s^j}$ ($i, j = 1, 2$). Denote the symmetric tensor formed by the coefficients l_{ij} by

$$M_{II} = \begin{pmatrix} l_{11} & l_{12} \\ l_{12} & l_{22} \end{pmatrix}. \qquad (B4)$$

Then the mean curvature of the surface is given by the mean of κ_1 and κ_2, the eigenvalues of the Weingarten transformation $M_{II} M_I^{-1}$,

$$H = \frac{1}{2}(\kappa_1 + \kappa_2) = \frac{1}{2} \text{Tr}(M_{II} M_I^{-1}) = \frac{1}{2} h^{ij} l_{ij} = -\frac{1}{2} \nabla_s \cdot \mathbf{n}, \qquad (B5)$$

where $\nabla_s = \mathbf{t}^1 \frac{\partial}{\partial s^1} + \mathbf{t}^2 \frac{\partial}{\partial s^2} = (I - \mathbf{n} \otimes \mathbf{n}) \nabla$ is the surface gradient operator.

A direct calculation using $h^{ij} = \mathbf{t}^i \cdot \mathbf{t}^j$, $\mathbf{t}^i = h^{im} \mathbf{t}_m$, and $l_{ij} = \frac{\partial \mathbf{t}_i}{\partial s^j} \cdot \mathbf{n}$ yields

$$\delta h^{ij} = -h^{im} \mathbf{t}^j \cdot \frac{\partial \delta \mathbf{q}}{\partial s^m} - h^{jm} \mathbf{t}^i \cdot \frac{\partial \delta \mathbf{q}}{\partial s^m}, \qquad (B6)$$

$$\delta l_{ij} = \frac{\partial^2 \delta \mathbf{q}}{\partial s^i \partial s^j} \cdot \mathbf{n} - \left(\frac{\partial \mathbf{t}_i}{\partial s^j} \cdot \mathbf{t}^m \right) \frac{\partial \delta \mathbf{q}}{\partial s^m} \cdot \mathbf{n}, \qquad (B7)$$

where we also used the fact that $\delta \mathbf{n} = -(\mathbf{n} \cdot \frac{\partial \delta \mathbf{q}}{\partial s^m}) \mathbf{t}^m$, which follows from $\delta \mathbf{n} = (\delta \mathbf{n} \cdot \mathbf{t}_m) \mathbf{t}^m$ and $\delta \mathbf{n} \cdot \mathbf{t}_m = -\mathbf{n} \cdot \delta \mathbf{t}_m$. It follows that

$$\delta H = \frac{1}{2} \delta h^{ij} l_{ij} + \frac{1}{2} h^{ij} \delta l_{ij} = -M_j^m \mathbf{t}^j \cdot \frac{\partial \delta \mathbf{q}}{\partial s^m} + \frac{1}{2}(\Delta_s \delta \mathbf{q}) \cdot \mathbf{n}, \qquad (B8)$$

where $M_j^m = l_{ij} h^{im}$ is the (j, m)th entry of $M_{II} M_I^{-1}$, and $\Delta_s = \nabla_s \cdot \nabla_s = h^{ij} \frac{\partial^2}{\partial s^i \partial s^j} + (\mathbf{t}^i \cdot \frac{\partial \mathbf{t}^j}{\partial s^i}) \frac{\partial}{\partial s^j}$ is Laplace-Beltrami operator.

To facilitate the calculation of the variation of the Willmore energy, we rewrite (B8) as

$$\delta H = \frac{1}{2} \Delta_s (\delta \mathbf{q} \cdot \mathbf{n}) + (\delta \mathbf{q} \cdot \mathbf{n})(2H^2 - K) + \nabla_s H \cdot \delta \mathbf{q}, \qquad (B9)$$

where $K = \kappa_1 \kappa_2$ is the Gaussian curvature. To see this, we decompose $\delta \mathbf{q}$ as $\delta \mathbf{q} = \delta \mathbf{q}^n + \delta \mathbf{q}^t$, where $\delta \mathbf{q}^n = (\delta \mathbf{q} \cdot \mathbf{n}) \mathbf{n}$ and $\delta \mathbf{q}^t = (\delta \mathbf{q} \cdot \mathbf{t}^k) \mathbf{t}_k$. Then

$$\frac{1}{2}(\Delta_s \delta \mathbf{q}^n) \cdot \mathbf{n} - M_j^m \mathbf{t}^j \cdot \frac{\partial \delta \mathbf{q}^n}{\partial s^m}$$
$$= \frac{1}{2} \Delta_s (\delta \mathbf{q} \cdot \mathbf{n}) - \frac{1}{2}(\delta \mathbf{q} \cdot \mathbf{n}) M_i^m M_m^i + (\delta \mathbf{q} \cdot \mathbf{n}) M_i^m M_m^i$$
$$= \frac{1}{2} \Delta_s (\delta \mathbf{q} \cdot \mathbf{n}) + \frac{1}{2}(\delta \mathbf{q} \cdot \mathbf{n}) M_i^m M_m^i$$
$$= \frac{1}{2} \Delta_s (\delta \mathbf{q} \cdot \mathbf{n}) + (\delta \mathbf{q} \cdot \mathbf{n})(2H^2 - K), \qquad (B10)$$

where we have used the fact that $M_i^m M_m^i = \text{Tr}(M_{II} M_I^{-1})^2 = 4H^2 - 2K$. For the tangential component $\delta \mathbf{q}^t$, a direct calculation yields

$$\frac{1}{2}(\Delta_s \delta \mathbf{q}^t) \cdot \mathbf{n} - M_i^m M_m^i \mathbf{t}^j \cdot \frac{\partial \delta \mathbf{q}^t}{\partial s^m} = \nabla_s H \cdot \delta \mathbf{q}^t = \nabla_s H \cdot \delta \mathbf{q}. \qquad (B11)$$

Equation (B9) follows from (B10) and (B11).

Finally, the variation of the Willmore energy is given by

$$\delta \int_\Sigma H^2 dA$$
$$= \int_\Sigma (2H \delta H + H^2 (\nabla_s \cdot \delta \mathbf{q})) dA$$
$$= \int_\Sigma (H \Delta_s (\delta \mathbf{q} \cdot \mathbf{n}) + (\delta \mathbf{q} \cdot \mathbf{n}) H(4H^2 - 2K)$$
$$+ \nabla_s \cdot (H^2 \delta \mathbf{q})) dA$$
$$= \int_\Sigma (\delta \mathbf{q} \cdot \mathbf{n})(\Delta_s H + 2H(H^2 - K)) dA$$
$$+ \int_{\partial \Sigma} (H \mathbf{m} \cdot \nabla_s (\delta \mathbf{q} \cdot \mathbf{n}) - (\delta \mathbf{q} \cdot \mathbf{n}) \mathbf{m} \cdot \nabla_s H$$
$$+ H^2 \mathbf{m} \cdot \delta \mathbf{q}) dl, \qquad (B12)$$

where we have applied the surface divergent theorem.

[1] T. Young, An essay on the cohesion of fluids, Philos. Trans. R. Soc. London **95**, 65 (1805).

[2] F. Neumann, *Vorlesungen über die Theorie der Capillarität* (B. G. Teubner, Leipzig, 1894).

[3] R. Pericet-Cámara, A. Best, H.-J. Butt, and E. Bonaccurso, Effect of capillary pressure and surface tension on the deformation of elastic surfaces by sessile liquid microdrops: An experimental investigation, Langmuir **24**, 10565 (2008).

[4] R. Pericet-Cámara, E. Bonaccurso, and K. Graf, Microstructuring of polystyrene surfaces with nonsolvent sessile droplets, ChemPhysChem **9**, 1738 (2008).

[5] Y. Xu, W. C. Engl, E. R. Jerison, K. J. Wallenstein, C. Hyland, L. A. Wilen, and E. R. Dufresne, Imaging in-plane and normal stresses near an interface crack using traction force microscopy, Proc. Natl. Acad. Sci. USA **107**, 14964 (2010).

[6] R. W. Style, R. Boltyanskiy, Y. Che, J. S. Wettlaufer, L. A. Wilen, and E. R. Dufresne, Universal Deformation of Soft Substrates Near a Contact Line and the Direct Measurement of Solid Surface Stresses, Phys. Rev. Lett. **110**, 066103 (2013).

[7] T. Kajiya, A. Daerr, T. Narita, L. Royon, F. Lequeux, and L. Limat, Advancing liquid contact line on visco-elastic gel substrates: Stick-slip vs. continuous motions, Soft Matter **9**, 454 (2013).

[8] R. Roman and J. Bico, Elasto-capillarity: Deforming an elastic structure with a liquid droplet, J. Phys.: Condens. Matter **22**, 493101 (2010).

[9] E. R. Jerison, Y. Xu, L. A. Wilen, and E. R. Dufresne, Deformation of an Elastic Substrate by a Three-Phase Contact Line, Phys. Rev. Lett. **106**, 186103 (2011).

[10] L. Limat, Straight contact lines on a soft, incompressible solid, Eur. Phys. J. E **35**, 134 (2012).

[11] R. W. Style and E. R. Dufresne, Static wetting on deformable substrates, from liquids to soft solids, Soft Matter **8**, 71 (2012).

[12] R. W. Style, L. Isa, and E. R. Dufresne, Adsorption of soft particles at fluid interfaces, Soft Matter **11**, 7412 (2015).

[13] R. W. Style, A. Jagota, C.-Y. Hui, and E. R. Dufresne, Elastocapillarity: Surface tension and the mechanics of soft solids, Annu. Rev. Condens. Matter Phys. **8**, 99 (2017).

[14] A. Marchand, S. Das, J. H. Snoeijer, and B. Andreotti, Contact Angles on a Soft Solid: From Young's Law to Neumann's Law, Phys. Rev. Lett. **109**, 236101 (2012).

[15] L. A. Lubbers, J. H. Weijs, L. Botto, S. Das, B. Andreotti, and J. H. Snoeijer, Drops on soft solids: Free energy and double transition of contact angles, J. Fluids Mech. **747**, R1 (2014).

[16] H. Zhao, A. P. Spann, and E. S. G. Shaqfeh, The dynamics of a vesicle in a wall-bound shear flow, Phys. Fluids **23**, 121901 (2011).

[17] H. Zhao and E. S. G. Shaqfeh, The shape stability of a lipid vesicle in a uniaxial extensional flow, J. Fluid Mech. **719**, 345 (2013).

[18] A. Farutin and C. Misbah, Symmetry breaking and cross-streamline migration of three-dimensional vesicles in an axial Poiseuille flow, Phys. Rev. E **89**, 042709 (2014).

[19] R. Capovilla, J. Guven, and J. A. Santiago, Deformations of the geometry of lipid vesicles, J. Phys. A: Math. Gen. **36**, 6281 (2003).

[20] X. Li, P. M. Vlahovska, and G. E. Karniadakis, Continuum- and particle-based modeling of shapes and dynamics of red blood cells in health and disease, Soft Matter **9**, 28 (2013).

[21] Z. Y. Luo and B. F. Bai, Dynamics of biconcave vesicles in a confined shear flow, Chem. Eng. Sci. **137**, 548 (2015).

[22] A. Bonito, R. Nochetto, and M. Pauletti, Dynamics of biomembranes: Effect of the bulk fluid, Math. Model. Nat. Phenom. **6**, 25 (2011).

[23] R. Skalak, A. Tozeren, R. P. Zarda, and S. Chien, Strain energy function of red blood cell membranes, J. Biophys. **13**, 245 (1973).

[24] A. Yazdani and P. Bagchi, Three-dimensional numerical simulation of vesicle dynamics using a front-tracking method, Phys. Rev. E **85**, 056308 (2012).

[25] T. Krüger, *Computer Simulation Study of Collective Phenomena in Dense Suspensions of Red Blood Cells under Shear* (Springer, Berlin, 2012).

[26] D. Abreu, M. Levant, V. Steinberg, and U. Seifert, Fluid vesicles in flow, Adv. Colloid Interface Sci. **208**, 129 (2014).

[27] A. Guckenberger and S. Gekle, Theory and algorithms to compute Helfrich bending forces: A review, J. Phys.: Condens. Matter **29**, 203001 (2017).

[28] W. Helfrich, Elastic properties of lipid bilayers: Theory and possible experiments, Z. Naturforsch. C **28**, 693 (1973).

[29] C. Huh and L. E. Scriven, Hydrodynamic model of steady movement of a solid/liquid/fluid contact line, J. Colloid Interface Sci. **35**, 85 (1971).

[30] E. B. Dussan V. and S. H. Davis, On the motion of a fluid-fluid interface along a solid surface, J. Fluid Mech. **65**, 71 (1974).

[31] R. G. Cox, The dynamics of the spreading of liquids on a solid surface. Part 1. Viscous flow, J. Fluid Mech. **168**, 169 (1986).

[32] D. Bonn, J. Eggers, J. Indekeu, J. Meunier, and E. Rolley, Wetting and spreading, Rev. Mod. Phys. **81**, 739 (2009).

[33] M. G. Velarde, Discussion and debate: Wetting and spreading science—quo vadis?, Eur. Phys. J.: Spec. Top. **197**, 1 (2011).

[34] T. Qian, X.-P. Wang, and P. Sheng, Molecular scale contact line hydrodynamics of immiscible flows, Phys. Rev. E **68**, 016306 (2003).

[35] W. Ren and W. E, Boundary conditions for moving contact line problem, Phys. Fluids **19**, 022101 (2007).

[36] W. Ren, D. Hu, and W. E, Continuum models for the contact line problem, Phys. Fluids **22**, 102103 (2010).

[37] W. Ren, P. H. Trinh, and W. E, On the distinguished limits of the Navier slip model of the moving contact line problem, J. Fluid Mech. **772**, 107 (2015).

[38] Z. Zhang and W. Ren, The distinguished limits of Navier slip model of moving contact line problem in Stokes flow, SIAM J. Appl. Math. **79**, 1654 (2019).

[39] Z. Zhang, S. Xu, and W. Ren, Derivation of a continuum model and the energy law for moving contact lines with insoluble surfactants, Phys. Fluids **26**, 062103 (2014).